THE JOURNAL OF BIOLOGICAL CHEMISTRY VOL. 284, NO. 16, pp. 10841–10854, April 17, 2009

Cloning and Characterization of Prisilkin-39, a Novel Matrix Protein Serving a Dual Role in the Prismatic Layer Formation from the Oyster *Pinctada fucata*[*] [S]

Received for publication, November 3, 2008, and in revised form, January 26, 2009 Published, JBC Papers in Press, February 19, 2009, DOI 10.1074/jbc.M808357200

Yawei Kong[‡], Gu Jing[‡], Zhenguang Yan[‡], Changzhong Li[‡], Ningping Gong[‡], Fangjie Zhu[‡], Dongxian Li[‡], Yaorun Zhang[‡], Guilan Zheng[‡], Hongzhong Wang[‡], Liping Xie[‡§1], and Rongqing Zhang[‡§2]

From the [‡]Institute of Marine Biotechnology, Department of Biological Sciences and Biotechnology, and [§]Protein Science Laboratory of the Ministry of Education, Tsinghua University, Beijing 100084, China

Molluscs form their shells out of $CaCO_3$ and a matrix of biomacromolecules. Understanding the role of matrices may shed some light on the mechanism of biomineralization. Here, a 1401-bp full-length cDNA sequence encoding a novel matrix protein was cloned from the mantle of the bivalve oyster, *Pinctada fucata*. The deduced protein (Prisilkin-39), which has a molecular mass of 39.3 kDa and an isoelectric point of 8.83, was fully characterized, and its role in biomineralization was demonstrated using both *in vivo* and *in vitro* crystal growth assays. Prisilkin-39 is a highly repetitive protein with an unusual composition of Gly, Tyr, and Ser residues. Expression of *Prisilkin-39* was localized to columnar epithelial cells of the mantle edge, corresponding to the calcitic prismatic layer formation. Immunostaining *in situ* and immunodetection *in vitro* revealed the presence of a characteristic pattern of Prisilkin-39 in the organic sheet and in sheaths around the prisms. Prisilkin-39 binds tightly with chitin, an insoluble polysaccharide that forms the highly structured framework of the shell. Antibody injection *in vivo* resulted in dramatic morphological deformities in the inner shell surface structure, where large amounts of $CaCO_3$ were deposited in an uncontrolled manner. Moreover, Prisilkin-39 strictly prohibited the precipitation of aragonite *in vitro*. Taken together, Prisilkin-39 is the first protein shown to have dual function, involved both in the chitinous framework building and in crystal growth regulation during the prismatic layer mineralization. These observations may extend our view on the rare group of basic matrices and their functions during elaboration of the molluscan shell.

The molluscan shell represents one of the most well known organo-mineral composites in the field of biologically controlled mineralization. It is a characteristically layered structure composed of calcium carbonate in the form of calcite, aragonite, or both, with small amounts of organic material (1). Although the integral organic macromolecules typically constitute less than 5 weight % of the biomineralized shell, they are, however, the major component responsible for different aspects of the shell formation process, including nucleation, polymorphism, orientation, morphology, and organization of growing crystallites, and they contribute in this way to the unique nano-scale structure and extraordinary properties of the shell (2, 3). Meanwhile, because of their exceptional self-assembling capacity and regulatory activity in the complex shell building process, shell matrices are also regarded as a source of bioactive molecules that can provide applied perspectives in the biomaterial and biomedical fields (4). Since the pioneering work of Sudo *et al.* (5), Miyamoto *et al.* (6), and Shen *et al.* (3), there has been much progress in investigations on molluscan shell matrix proteins in the last decade (for review see Refs. 7–9). However, information on the structure and role of the organic matrix is still limited, and the detailed molecular mechanism of shell mineralization holds much to be discovered. This is presumably due to problems associated with separation and purification of these biomacromolecules (10, 11), as well as the lack of suitable *in vivo* or *in vitro* models to study them.

The shell of the bivalve oyster consists of two mineralized layers as follows: an inner nacreous and an outer prismatic layer. Based on a comparative analysis of currently known molluscan shell proteins according to the different shell layers in which they are present, the interesting phenomenon of an unbalanced protein distribution pattern has been discovered. It mainly embodies the fact that all of the extremely acidic shell proteins ($pI < 4.5$) are preferentially associated with the calcitic prismatic layer rather than the aragonitic nacreous layer (4, 5, 12–16). Acidic matrix proteins are believed to be the major components in the soluble fraction of the shell matrix, and they exert effective control over the crystal growth because of their cation-binding capacity (17–20). Previous reports have revealed that these highly acidic proteins can decide the calcium carbonate polymorphism *in vitro* (2, 12, 21, 22). One striking example is Aspein (12, 23), which acts as a crystal nucleator to induce calcite precipitation using the mechanism of ionotropy, and it is therefore crucial for the formation of the prismatic layer. In contrast, basic matrix proteins exclusively associated with the prismatic layer have been far less studied. Until now, only three proteins, including the Shematrin family (24), KRMPs (25), and tyrosinase-like protein 2 (26), have been

* This work was supported by the National High Technology Research and Development Program of China Grants 2006AA09Z441 and 2006AA09Z413 and the National Natural Science Foundation of China Grants 30530600, 30221003 and U0831001 (Joint Fund with Guandong).

[S] The on-line version of this article (available at http://www.jbc.org) contains Figs. S1 and S2.

The nucleotide sequence(s) reported in this paper has been submitted to the GenBank™/EBI Data Bank with accession number(s) EU921665.

[1] To whom correspondence may be addressed. Tel.: 86-10-62772899; Fax: 86-10-62772899; E-mail: lpxie@mail.tsinghua.edu.cn.

[2] To whom correspondence may be addressed. Tel.: 86-10-62772899; Fax: 86-10-62772899; E-mail: rqzhang@mail.tsinghua.edu.cn.

reported and characterized only at the genetic level. It has been speculated that they play key roles in the process of framework construction on the basis of information from the primary structure. However, no direct proof has been provided.

In the process of molluscan shell building, two different kinds of polymorphic crystals are precipitated at specific sites of the shell layers and arranged in a highly ordered manner, finally resulting in the exquisite architecture. What is the key link for their precisely controlled precipitation? The reason for the transition of the shell layers is an intriguing question, but the answer remains unclear. One point to mention is the previous finding that an organic sheet, sandwiched between the prismatic layer and the nacreous layer, has been demonstrated by immunohistochemistry (27, 28). Because the organic sheet interacts simultaneously with both calcified layers as the only intermedium in-between, it is considered to be, to some extent, responsible for particular steps during the polymorphic transition. However, little is known about this organic sheet as yet. It is so thin (10–50 μm) that no matrix protein within this layer has ever been successfully characterized. In this study, we report the cloning and characterization of a matrix protein named Prisilkin-39, which is proven to be the first protein localized in the organic sheet, as well as to be a novel basic protein associated with the prismatic layer from the oyster *Pinctada fucata*. The nature and function of Prisilkin-39 in the shell mineralization process were elucidated by a combination of biochemical and genetic analyses. Our results demonstrated that Prisilkin-39 likely serves a dual role, both participating in the process of organic framework construction and aragonite-specific inhibition during the calcitic prismatic layer mineralization.

EXPERIMENTAL PROCEDURES

Animals—Rapidly growing specimens (25–35 g wet weight) of *P. fucata* were collected from the Guofa Pearl Farm in Beihai, Guangxi Province, China. The oysters were maintained in aerated artificial seawater (Sude Reef Sea Salt, 3% at 25 °C) for 3 days prior to experimentation.

RNA Purification and Complementary DNA Synthesis—Total RNA was extracted from the mantle tissue of *P. fucata* using an RNA isolation kit, RNAzol (Biotecx Laboratories, Inc.) according to the manufacturer's instructions. The integrity of RNA was determined by fractionation on 1.2% formaldehyde-denatured agarose gel and staining with ethidium bromide. The quantity of RNA was determined by measuring $A_{260\ nm}$ with an Utrospec 3000 UV-visible spectrophotometer (Amersham Biosciences). Approximately 2 μg of mantle total RNA was used as template for first-strand cDNA synthesis using the BD PowerScript™ Reverse Transcriptase (Clontech) for subsequent rapid amplification of cDNA ends (RACE)[3] reactions.

Construction of Mantle cDNA Library—Poly(A)$^+$ RNA from the mantle tissue of *P. fucata* was extracted using the poly(A) tract mRNA isolation system (Promega Corp.). Double-stranded cDNA was generated using ~5 μg of poly(A)$^+$ RNA. The cDNA was subsequently ligated into the Uni-ZAP XR Vector and packaged with the Gigpack III Gold extract (Stratagene).

Rapid Amplification of cDNA Ends and Sequence Analyses—3′-RACE and 5′-RACE were carried out with a BD SMART™ RACE cDNA amplification kit and Advantage 2 cDNA polymerase mix (Clontech) according to the manufacturer's instructions. 3′-RACE was performed using the first-strand cDNA and the primer pair of UPM (Clontech) and a degenerate sense primer YGS-F1 (5′-GG*N* TA*Y* GG*N* GG*N* TA*Y* *N*G-3′, *N* = A/G/C/T; *Y* = C/T). The primer YGS-F1 was designed based on the amino acid sequence GYGGYG containing the repetitive motif GYGG of KRMP, the prismatic layer framework matrix protein of *P. fucata.* Full-length cDNA was amplified by 5′-RACE using the primer pair of UPM and a gene-specific antisense primer YGS-R1 (5′-AAC TAT ACC CTG AAC GCA TTC CAC C-3′) designed from the nucleotide sequence of the cDNA fragment determined by 3′-RACE. All PCR-amplified products were selectively purified with Wizard PCR Prep DNA purification system (Promega) and subcloned into the pMD 19-T vector (Takara) for sequencing. To confirm cloning and sequencing accuracy, the entire cDNA was re-amplified with high fidelity polymerase (Takara) and the *P. fucata* mantle cDNA library as template, using the set of primers of the gene-specific primer YGS-F2 (5′-TTC ACT GCA GTT TCG AAC TAC-3′) and T7 (reverse primer, corresponding to the T7 promoter on the Uni-ZAP vector). The purified PCR products were subcloned into pMD 19-T vector followed by re-sequencing.

Gene Expression Analysis by RT-PCR—Total RNA was isolated as described above from different tissues, including the mantle edge, the mantle pallial, gonad, foot, gill, hemocytes, viscus, and adductor muscle of adult individual of *P. fucata*. Equal quantities (1 μg) of total RNA from different tissues were reverse-transcribed into cDNA with Superscript III reverse transcriptase (Invitrogen). RT-PCR was conducted using the primer pairs of YGS-T1 (5′-ATG CGT TCA GGG TAT AGT TAT TAC AGC-3′) and YGS-T2 (5′-TAC TAC CAG AAC TGT AAT ATG ATG G-3′), and gapdhF (5′-GCC GAG TAT GTG GTA GAA TC-3′) and gapdhR (5′-CAC TGT TTT CTG GGT AGC TG-3′) for amplification of Prisilkin-39 and GAPDH (included as a positive control for cDNA preparations) gene fragment, respectively. To avoid false-positive results and detect the cross-contamination of the samples, a negative control was performed in the absence of cDNA template. All PCR products were subcloned and verified by sequencing.

In Situ Hybridization—In situ hybridization of Prisilkin-39 mRNA was carried out on frozen sections of the mantle tissue that had been fixed in 4% paraformaldehyde containing 0.1% diethyl pyrocarbonate (Sigma) overnight. The digoxigenin-labeled probe was generated from the 361-bp fragment amplified with the primer pair of YGS-T1 and YGS-T2 by using a High Prime DIG random labeling kit (Roche Applied Science). The procedures of hybridization were mainly performed as described previously with some modifications (29).

[3] The abbreviations used are: RACE, rapid amplification of cDNA ends; anti-Prisilkin-39, specific antibody against Prisilkin-39; BSA, bovine serum albumin; RT, reverse transcription; PBS, phosphate-buffered saline; ELISA, enzyme-linked immunosorbent assay; GAPDH, glyceraldehyde-3-phosphate dehydrogenase; SEM, scanning electron microscope; ESM, EDTA-soluble matrix; EISM, EDTA-insoluble matrix.

Preparation of Polyclonal Antibodies against the Recombinant Prisilkin-39—Construction of expression vector pPIC9/Pf-Prisilkin-39 was performed as described in the *Pichia* expression kit (Invitrogen) manual. Recombinant Prisilkin-39 with a His tag at the N terminus was overexpressed in yeast, *Pichia pastoris* GS115, after 2 days of induction, and then purified from the medium by chromatography on DEAE-Sepharose Fast Flow and Ni-NTA affinity column (Amersham Biosciences). Elution fractions containing recombinant Prisilkin-39 detected by SDS-PAGE were concentrated and desalted by ultrafiltration (Millipore, cut-off 5 kDa) against 10 mM Tris/HCl buffer, pH 7.4. Polyclonal antibodies against Prisilkin-39 (anti-Prisilkin-39) were raised in New Zealand rabbits following standard immunization procedures and then affinity-purified from nitrocellulose membrane as described previously (30). The titer was determined by standard enzyme-linked immunosorbent assay (31). In addition, the specificity of the antibodies was tested on Western blots against the purified protein, the polyhistidine, and the EDTA-insoluble matrix extracted from the entire shell of *P. fucata*.

Shell Preparation and Matrix Extraction—Cleaned shells of *P. fucata* were immersed in 5% sodium hydroxide for 12 h and subsequently rinsed in distilled water to avoid possible contamination of the shell matrix by soft tissues that could have adhered to the inner surface of nacre. The two layers of the shells, the outer calcitic prismatic layer and the inner aragonitic nacreous layer, were separated mechanically by abrasion before air-drying. Their respective fragments were pulverized (30 g, particle size <100 μm) and then decalcified with 0.5 M sodium EDTA (Merck) for 60 h at 4 °C with continuous stirring. For extraction of the soluble matrix, the supernatant was collected by centrifugation at 13,000 rpm for 30 min at 4 °C, then desalted by ultrafiltration (Amicon, YM50) under nitrogen, and lyophilized. The pellets were thoroughly rinsed with water and treated with denaturing solution (30 mM Tris/HCl, pH 8.0, 1% SDS, 10 mM dithiothreitol) at 100 °C for 15 min. After a short centrifugation, the denatured samples were ready to be applied on 12% SDS-polyacrylamide gels. Gels were either stained with Coomassie Brilliant Blue or electroblotted onto a polyvinylidene difluoride membrane. Extracts of the entire shell were also obtained in the same manner. The amount of the protein was measured by a BCA assay kit (Pierce).

Detection of Native Prisilkin-39 in Different Shell Extracts and Tissues—Analysis of the existence of native Prisilkin-39 in EDTA extracts of the prismatic layer and the nacreous layer of *P. fucata* was conducted by a combination of ELISA, dot-blot testing, and Western blotting, using affinity-purified polyclonal antibodies. For the dot-blot test, solutions containing the extracts of shell matrix were serially diluted with the same buffer and then vacuum-blotted onto a polyvinylidene difluoride membrane. The membrane was incubated with the antibodies and then treated as a normal blot. For ELISA, known amounts (100 pg to 3 ng of Prisilkin-39) were used as a standard. The tests were repeated three times in triplicate. Tissues, *i.e.* mantle, gill, gonad, viscus, foot, and adductor muscle, were homogenized, and the total proteins were extracted using TRIzol Reagent (Invitrogen) according to the manual. Homolymph and extrapallial fluid were extracted directly from oyster *P. fucata* by sucking the fluid gently using a sterile syringe. Protein samples with an equal quantity (30 μg) were run on an SDS-polyacrylamide gel and transferred to nitrocellulose membrane using the Multiphor II Western blotting system (Amersham Biosciences). Purified polyclonal antibodies were used at dilutions of 1:100, and alkaline phosphatase-labeled goat anti-rabbit antibody (Calbiochem) at 1:2000. The blot was finally visualized with nitro blue tetrazolium/5-bromo-4-chloro-3-indolyl phosphate (Roche Applied Science).

In Situ Immunofluorescence Location of Native Prisilkin-39—Immunofluorescence staining was performed according to Nudelman *et al.* (32) with minor modifications. After being washed and sonicated in distilled water for 10 min, a cross-section of the shell was incubated in a solution of 0.5 M EDTA, pH 8.0, containing 4% formaldehyde and 0.5% cetylpyridinium chloride at room temperature with gentle shaking for 3 days. After complete decalcification, the samples were thoroughly washed with Milli-Q water and blocked in 10% goat serum for 2 h. The samples were then incubated in serum containing polyclonal antibodies produced against recombinant Prisilkin-39 or preimmune serum. In both cases the serum was diluted 1:50 in PBS and contained bovine serum albumin 0.25% w/v (Sigma) to block nonspecific binding. After washing with PBS containing 0.05% Tween 20 for 5 min, the second antibody, rhodamine-conjugated goat anti-rabbit (Santa Cruz Biotechnology, diluted 1:1000 in PBS) was applied to the samples for 30 min. Rhodamine-labeled samples were washed with PBS, rinsed in water, and examined with differential interference contrast microscopy and fluorescence microscopy (Leica, DMIRB).

Chitin Binding Assay—Chitin binding assays were done as described by Inoue *et al.* (33) with some modifications. Recombinant Prisilkin-39 or BSA (each 30 μg) as a negative control was dissolved in 50 μl of 0.5% ammonium bicarbonate, and the resulting solution was incubated with 5 mg of chitin (Wako) that had previously been equilibrated with 0.5% ammonium bicarbonate for 20 h at 4 °C in an Eppendorf tube. After removal of the solution by centrifugation, the insoluble mixture was successively washed with 200 μl each of distilled water and 0.2 M NaCl. Each washing was desalted by ultrafiltration (Millipore, 5-kDa cutoff) and lyophilized, and freeze-dried proteins were resuspended directly in 15 μl of Laemmli sample buffer. The final insoluble residue was boiled in 30 μl of 2% (w/v) SDS containing 20% (v/v) 2-mercaptoethanol for 10 min, and then the supernatant was separated by centrifugation at 12,000 rpm for 5 min. Each washing or supernatant was subjected to SDS-PAGE on a 12% gel under reducing conditions. After electrophoresis, the gel was stained with Coomassie Brilliant Blue.

In Vitro Crystallization Assay—Two types of crystallizing solutions were prepared to investigate the effect of Prisilkin-39 on the morphology and polymorphism of calcium carbonate crystals. Saturated calcium bicarbonate solution for calcite crystallization was prepared according to Xu *et al.* (34). A stirred aqueous suspension of calcium carbonate was aerated with CO_2 for 4 h, and the excess solid calcium carbonate was removed by filtration (0.2 μm). An aragonitic crystallizing solution was obtained by the addition of 50 mM magnesium chloride to the former solution. Crystallization experiments were car-

ried out by adding samples to the freshly prepared filtrate on siliconized glass slides at 20 °C. The slides were placed into a sealed box with a sheet of wet paper to prevent evaporation. After 24 h, the crystallization solution was removed, and the crystals were stored in a desiccator for characterization.

Inhibition of Calcium Carbonate Precipitation and Calcium Binding Assay—The effect of Prisilkin-39 on calcium carbonate precipitation from its supersaturated solution was examined according to the method of Suzuki *et al.* (13). Briefly, sample solution (10 μl) was mixed with 100 μl of 30 mM $NaHCO_3$, pH 8.5. After the addition of 100 μl of 30 mM $CaCl_2$ to the mixed solution, the formation of $CaCO_3$ precipitates was monitored by recording the turbidity. Changes in the turbidity of the solutions were measured every minute for 5 min by the absorbance at 570 nm using a spectrophotometer. The calcium-binding capacity of Prisilkin-39 was analyzed according to the Stains-All method (35). Gels were run, extensively washed with 25% isopropyl alcohol, and then stained in the dark for 4 days with 0.0025% Stains-All, 25% isopropyl alcohol, 7.5% formamide, and 30 mM Tris base, pH 8.8. Calmodulin, a calcium-binding protein (36), was used as a positive control. A calcium-dependent electrophoretic shift assay was carried out according to the method of Burgess *et al.* (37).

Protein Labeling with Rhodamine and Crystal Binding Experiment—Protein labeling with rhodamine and protein-crystal binding experiments were performed as described previously (38).

In Vivo Antibody Inhibition Assay—The purified antibodies were injected into the extrapallial space through the zone of the mantle tissue outside the pallial line at the dosage of 0.5 μg (low dosage) and 1 μg (high dosage) per g of wet weight per day. Five specimens in each group were sacrificed 3 days after antibody injection. The shells were separated, washed with Milli-Q water, and immersed in 5% NaOH for 12 h to remove organic components attached to the inner surface. The shells were thoroughly washed with Milli-Q water, air-dried, gold-coated, and observed under a SEM.

Crystal Characterization—For morphological observation and identification of the induced crystals, Raman spectra, SEM, and fluorescence microscopy were used. The Raman spectra of the crystals were recorded with an excitation wavelength of 514 nm, which was provided by an argon laser limited to 4.6-milliwatt power. The spectra were scanned three times for 20 s in the range of 100–1400 cm^{-1} with a Renishaw RM2000 spectrometer. The scanning electron micrographs were obtained using a FEI Sirion2000 SEM equipped with an energy-dispersive x-ray spectroscopy system for element analysis of crystals. For rhodamine-labeled crystals, a fluorescence microscope (Leica, DMR) was used.

RESULTS

Isolation and Sequence Analysis of cDNA for Prisilkin-39—A fragment of 1000 bp was obtained by the 3′-RACE procedure with degenerate primer YGS-F1. Subsequent sequencing analysis revealed that the degenerate primer YGS-F1 had annealed to the sequence of cDNA encoding GYGGYS. Based on this 3′ sequence, a gene-specific antisense primer YGS-R1 was synthesized, and the full-length cDNA was obtained by the 5′-RACE procedure. To confirm the sequence expected from the results of 3′-RACE and 5′-RACE, another amplification of the full-length cDNA was performed using the *P. fucata* mantle cDNA library as a template. A positive cDNA clone YGS7 was obtained, and the final confirmed sequence, including the poly(A) tail, turned out to be 1401 bp in length (Fig. 1). It contains a 59-base 5′-untranslated sequence, an open reading frame consisting of 1218 bp, an in-frame stop codon TAA, and a 121-base 3′-untranslated sequence. The context of the first start codon at nucleotide 60, with a purine (A) three nucleotides upstream, is compatible with the Kozak consensus sequence for initiation of transcription in eukaryotic species (39, 40). Within this cDNA sequence, a putative polyadenylation signal AATAAT is recognized at the nucleotide position 1305, which is 76 nucleotides upstream of the poly(A) tail.

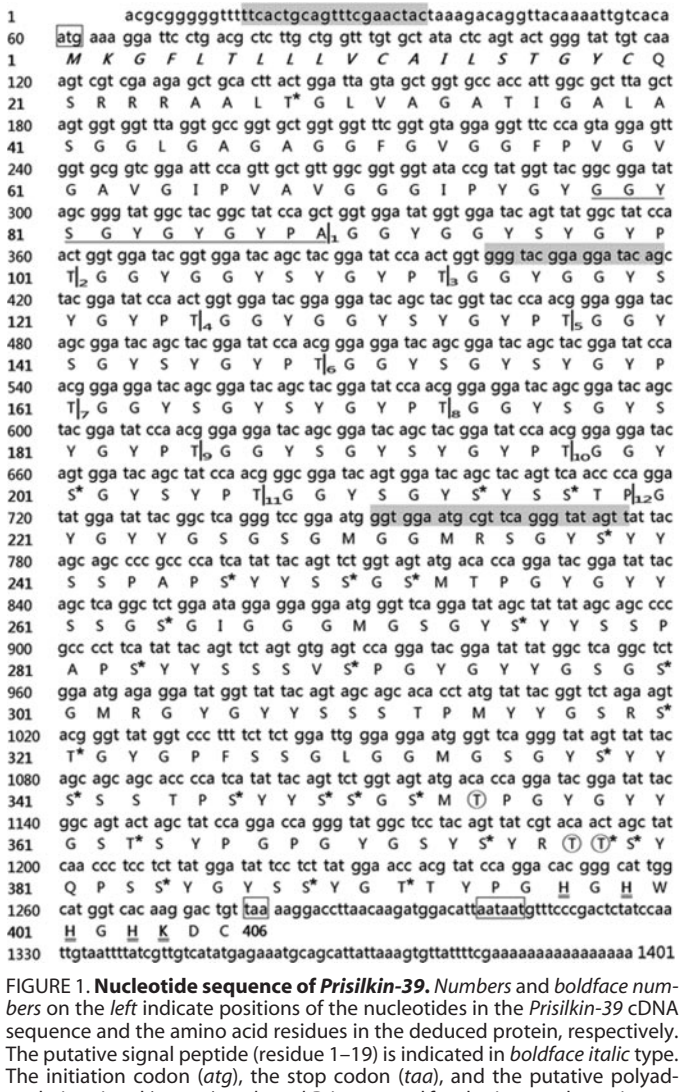

FIGURE 1. **Nucleotide sequence of *Prisilkin-39*.** *Numbers* and *boldface numbers* on the *left* indicate positions of the nucleotides in the *Prisilkin-39* cDNA sequence and the amino acid residues in the deduced protein, respectively. The putative signal peptide (residue 1–19) is indicated in *boldface italic* type. The initiation codon (*atg*), the stop codon (*taa*), and the putative polyadenylation signal (*aataat*) are *boxed*. Primers used for cloning are shown in *gray shading*. Protein sequence of Prisilkin-39 contains 12 tandem repeats; the first repeat is *underlined*, and the last amino acid residue of each repeat is indicated by a *vertical line* and *numbered 1–12*. Four histidine residues and one lysine residue in the C terminus are *double underlined*. The putative phosphorylation sites are shown by *asterisks*, and the three threonine residues representing possible *O*-glycosylation sites are *circled*.

Characterization of Deduced Amino Acid Sequence of Prisilkin-39—The deduced protein Prisilkin-39 encompasses 406 amino acid residues and has a calculated molecular mass of 39.3 kDa before any post-translational modification. Prisilkin-39 is characterized by high proportions of Gly (29.7%), Tyr (23.3%), and Ser (18.6%), which together accounted for more than 70% of the total amino acid residues (Table 1). In addition, the amino acid composition of Prisilkin-39 is also comparable with that of crude matrix proteins from the prismatic layer of *P. fucata* (41). In contrast to many other shell matrix proteins singularly enriched in Asp and Glu residues (12–16), the occurrence of these acidic amino acids in Prisilkin-39 is markedly low, with only one Asp residue. Thus, Prisilkin-39 belongs to the rare group of basic matrix proteins with a theoretical pI of 8.83.

TABLE 1
Amino acid composition of Prisilkin-39, KRMP, and Shematrin-1

Amino acid	Prisilkin-39		KRMP-1		Shematrin-1	
	Residues	mol %	Residues	mol %	Residues	mol %
Gly	115	29.72	14	17.28	129	38.05
Tyr	90	23.26	13	16.05	48	14.16
Ser	72	18.60	3	3.7	29	8.55
Pro	29	7.49	3	3.7	14	4.13
Thr	23	5.94	1	1.23	8	2.36
Ala	13	3.36	1	1.23	21	6.19
Met	8	2.07	0	0	1	0.29
Val	8	2.07	0	0	29	8.55
Arg	7	1.81	1	1.23	5	1.47
leu	5	1.29	4	4.94	16	4.72
His	4	1.03	5	6.17	1	0.29
Ile	4	1.03	1	1.23	13	3.83
Phe	3	0.78	1	1.23	11	3.24
Gln	2	0.52	0	0	4	1.18
Asp	1	0.26	4	4.94	1	0.29
Lys	1	0.26	14	17.28	3	0.88
Trp	1	0.26	8	9.88	0	0
Cys	1	0.26	6	7.41	0	0
Asn	0	0.00	2	2.47	6	1.77
Glu	0	0.00	0	0	0	0
Total	387		101		339	
M_r	39,323		9798		31,912	
pI	8.83		9.58		9.13	

Another characteristic feature of the Prisilkin-39 sequence lies in its modular structure, consisting of a signal peptide, a short N-terminal alanine-rich hydrophobic region, two highly repetitive regions, and a C-terminal histidine-rich basic tail (Fig. 2*A*). The first 19 amino acids apparently include a signal peptide, which shares high similarity with the signal peptides of MSI31 (5) and MSI7 (42), two matrix proteins involved in the prismatic layer formation of *P. fucata*, as well as that of Aspein (12) and the Asprich family (16), the extremely acidic matrix proteins of the prismatic layer of *P. fucata* and *Atrina rigida*. Considering the high composition of hydrophobic amino acids in the first 60 residues of the mature protein (Fig. 2*B*, *arrowheads*), the hydropathy of Prisilkin-39 was further examined using the method of Kyte and Doolittle available on line. The analysis revealed that the only hydrophobic region of the molecule is located at the N terminus, corresponding to residues 20–77 in the alanine-rich region (Fig. 2*B*). Following this region, almost 80% of the length of the Prisilkin-39 sequence is occupied by two consecutive regions termed GYS region I and GYS region II (Fig. 2, *C* and *D*). They are arranged in tandem with highly conserved repeats, making Prisilkin-39 one of the most repetitive molluscan shell proteins we know. GYS region I consists of 12 repetitive sequence elements, 10 of which are GGY(G/S)GY(G/S)YGYP(T/A). These elements share high degrees of sequence similarity, suggesting that they are likely to have similar folding structures. Similarly, GYS region II is also characterized by random repetitive elements, which are dominated by Gly-Tyr, Tyr-Ser, Tyr-Tyr, and Gly-Ser dipeptides. However, there seems to be no regularity in terms of the arrangement of these different dipeptides in this section, making GYS region II less repetitive than GYS region I. The two repeated regions are followed by a stretch of 10 amino acids rich in polar residues. Four histidine residues and one lysine residue are densely located in the C terminus of Prisilkin-39. This basic tail shares some similarity with that of the Shematrin protein family (24). It is possible that in the extrapallial fluid, pH 7.4, where matrix assembly and shell mineralization occur (3), the side chains of these residues are inclined to be positively charged and therefore able to interact with carbonate

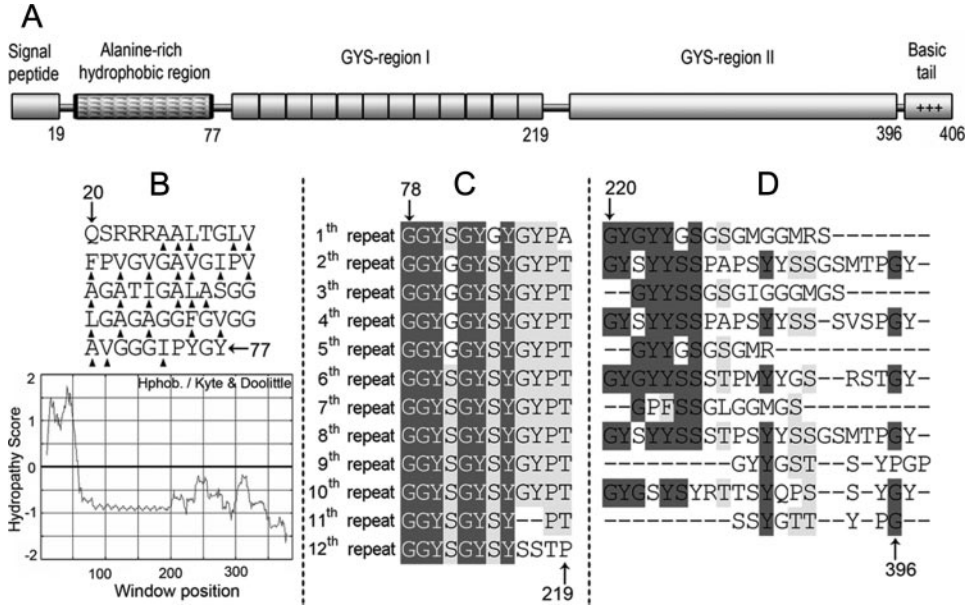

FIGURE 2. **Schematic representation of Prisilkin-39.** *A,* schematic representation of the modular structure of Prisilkin-39. The protein includes a signal peptide, a short N-terminal alanine-rich hydrophobic region (residues 20–77), two highly repetitive regions, GYS region I (residues 78–219) and GYS region II (residues 220–396), and a C-terminal histidine-rich basic tail (residues 397–406). *B,* sequence of the alanine-rich hydrophobic region (*upper compartment*) and the corresponding hydrophobicity plot for Prisilkin-39 (*lower compartment*). Amino acids with high hydropathy scores are indicated by *arrowheads*. Analysis of hydrophobicity was done using the method of Kyte and Doolittle (window = 19). *C,* sequence alignment of the 12-fold tandem repeats of a consensus sequence in GYS region I. Consensus amino acid residues are *shaded*, and the identical glycine and tyrosine residues are *highlighted*. *D,* sequence alignment of GYS region II. The *vertical arrow* and *number* designate the amino acid range of each region in *B–D*.

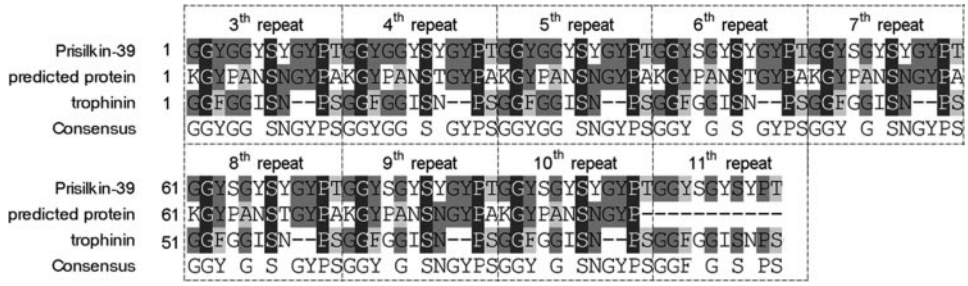

FIGURE 3. **Alignment of repeats 3–11 of Prisilkin-39 with those of two similar tandem repeated proteins.** The proteins used in the figure are the predicted protein from *O. lucimarinus CCE9901* (residues 55–149), NCBI accession number ABO98608, and the trophinin protein from *Mus musculus* (residues 894–990), NCBI accession number NM001002272. Amino acids are numbered on the *left,* and *gaps* are indicated by (−). Identical residues are *highlighted* and *shaded in black*, and other conserved residues are *shaded*.

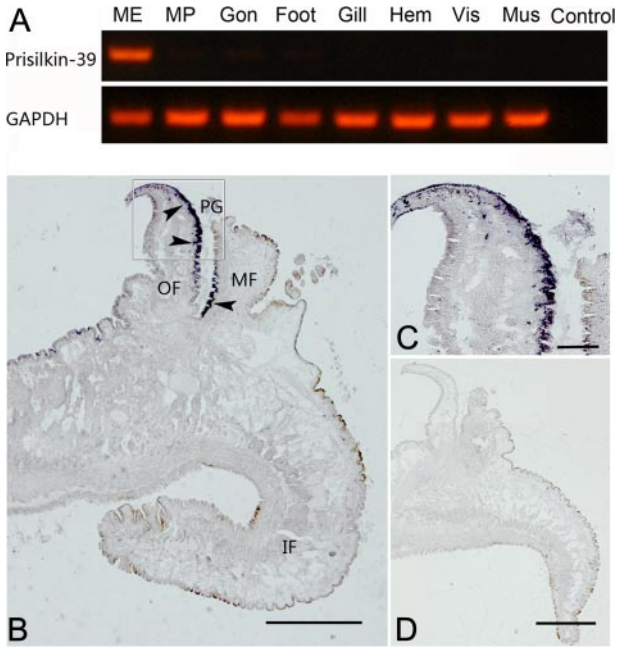

FIGURE 4. **Gene expression pattern of *Prisilkin-39* and its location to the columnar epithelium of the mantle tissue.** *A,* tissue-specific gene expression of *Prisilkin-39* by RT-PCR analysis. Total RNA was extracted from mantle edge (*ME*), mantle pallial (*MP*), gonad (*Gon*), foot, gill, hemocytes (*Hem*), viscus (*Vis*), and adductor muscle (*Mus*). The housekeeping gene GAPDH was used as a positive control. Following reverse transcription, PCR was performed using primer sets for Prisilkin-39 and GAPDH presented under "Experimental Procedures." *B,* detection of Prisilkin-39 mRNA in the mantle of *P. fucata* by *in situ* hybridization. Hybridization signals (*dark purple*) in the inner epithelial cells of the outer fold and the outer epithelial cells of the middle fold are indicated by *arrowheads*. *OF,* outer fold; *MF,* middle fold; *IF,* inner fold; *PG,* periostracal groove. *Bar*, 500 μm. *C,* enlargement of the box in *B*. *Bar,* 100 μm. *D,* control section stained with a sense probe. *Bar*, 500 μm.

ions and negatively charged amino acid residues in other acidic proteins (14).

Further bioinfomatics analysis of the Prisilkin-39 sequence suggests that some serine and threonine residues in Prisilkin-39 may either be phosphorylated or *O*-glycosylated (as indicated in Fig. 1), a feature commonly found with proteins associated with mineralized tissues (1). Strikingly, three potential *O*-glycosylation sites and 24 phosphorylation sites out of 28, according to NetOGlyc3.1 (43) and NetPhos2.0 (44), respectively, are densely distributed in GYS region II. This may indicate that GYS region II is likely to have a more flexible and complicated folding structure, as it is more sensitive to post-translational modifications than the GYS region I.

The Blastp (protein-protein BLAST) search (45) against GenBank™ showed no significant homology of Prisilkin-39 with any other known protein. A low resemblance to Prisilkin-39 was found in a predicted protein from *Ostreococcus lucimarinus* and a mouse protein trophinin (46) (Fig. 3). Both proteins contain a conserved glycine-rich unit, which is repeated in tandem as in Prisilkin-39 10 and 13 times, respectively. However, there has been no indication of any known functions.

Gene Expression Analyses—The expression of *Prisilkin-39* was tested in several target tissues of *P. fucata* by RT-PCR (Fig. 4*A*), with expression being detected only in the mantle edge, corresponding to the prismatic calcite shell layer, but not in the mantle pallial corresponding to the nacreous aragonite layer and nor in any other tissues (supplemental Fig. 1). To determine the more precise expression sites of Prisilkin-39 mRNA in the mantle edge of *P. fucata*, *in situ* hybridization was performed with frozen sections of the mantle. Expression of *Prisilkin-39 in situ* was localized to the inner epithelial cells of the outer fold, and the outer epithelial cells of the middle fold at the bottom of the periostracal groove (Fig. 4, *B* and *C*). In contrast, no hybridization signal was detected at the dorsal mantle or in the inner fold. Hybridization with a control probe gave no significant signals (Fig. 4*D*). Furthermore, it is noteworthy that this expression profile was partially similar to that of Prismalin-14 (13) and KRMP (25), two proteins from the prismatic layer of *P. fucata*, suggesting the probable involvement of Prisilkin-39 in the process of prismatic layer formation.

Prisilkin-39 in Extracts of Nacre and Prisms of P. fucata—Biochemical analyses were performed to investigate whether native Prisilkin-39 is present in the prismatic or nacreous layer of *P. fucata* or in both. Yeast, an increasingly used eukaryotic expression system, was chosen to yield recombinant proteins because of its advantages in protein folding and post-translational modification in this study. The recombinant form of the Prisilkin-39 protein was produced in *P. pastoris* GS115 cells and then purified on nitrilotriacetic acid beads. Polyclonal antibodies raised against recombinant Prisilkin-39 were used for immunodetection of native Prisilkin-39 in fractions of EDTA-soluble matrix (ESM) and EDTA-insoluble matrix (EISM) of the shell of *P. fucata*. The reactions were carried out using ELISA and immune dot blot assay. As shown in Fig. 5, Prisilkin-39 was only detected in the EISM but not in the ESM of the shell. According to previous reports on matrix proteins (47–50), EISM proteins were conventionally believed to be responsible for the construction of the structural organic framework and the physical properties of the shell during calcification. Therefore, it is logical to assume that Prisilkin-39 exists as a framework component in the prismatic shell layer considering its presence pattern and amino acid composition (Gly/Tyr-rich).

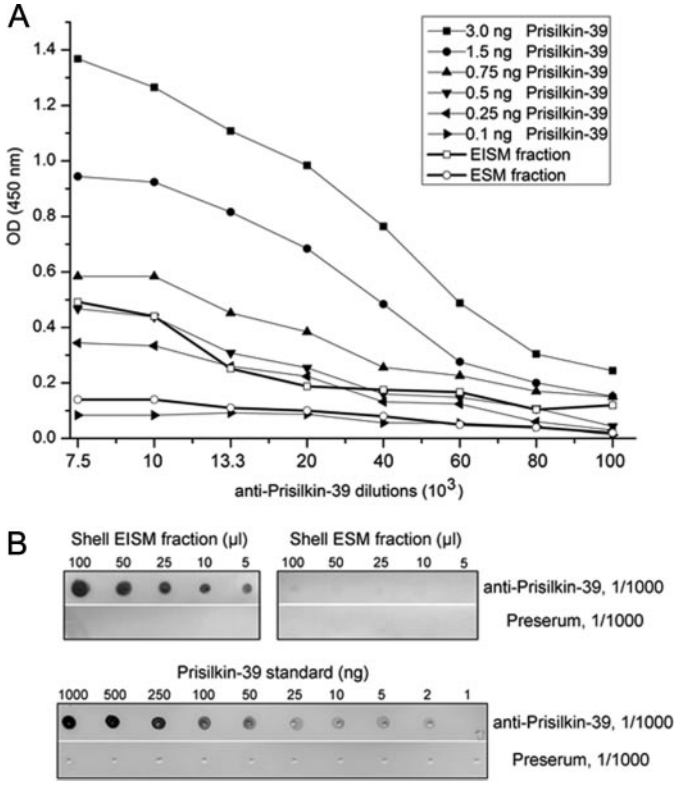

FIGURE 5. **Detection of native Prisilkin-39 in different shell extracts.** The purified anti-Prisilkin-39 antibody was tested against EDTA-soluble matrix (*ESM*) and EDTA-insoluble matrix (*EISM*) of the shell of *P. fucata*, via ELISA (*A*) and dot immune blot assay (*B*). For more information, see "Experimental Procedures." The extracts were compared with known amounts of recombinant Prisilkin-39, which were serially diluted in EDTA and treated as a positive control. Both the ELISA curve (*A*) and the blot (*B*) show that strong signals are detected in the EISM but not in the ESM of the shell.

In addition, the presence of Prisilkin-39 in the prismatic shell layer was further investigated and verified with SDS-PAGE and Western blotting on EDTA extracts from separated nacre and prisms. Coomassie Brilliant Blue staining of the gels revealed the existence of numerous discrete thin bands together with the smeared background (Fig. 6*A*), which exhibited the peculiar behavior of total shell proteins. All extracts showed distinctively different patterns, and a number of matrix proteins were poorly resolved on acrylamide gels using Coomassie Blue or Silver nitrate staining (data not shown). Meanwhile, Stains-All stained gel images corresponding to the samples shown in Fig. 6*A* showed that both the recombinant Prisilkin-39 and the prism EISM extracts negatively stained pink, and accordingly it provides evidence that native Prisilkin-39 is not an abundant phosphoprotein in the prism EISM extracts (Fig. 6*B*). Western blot results showed that Prisilkin-39 was detected exclusively in the EDTA-insoluble fractions of the prisms after being treated with denaturing solution at 100 °C for 15 min. Neither the fractions of nacre nor the EDTA-soluble fraction of the prisms showed any reaction with anti-Prisilkin-39 (Fig. 6*C*). The biochemical location pattern of Prisilkin-39 did, however, coincide with the results of previous gene expression analysis. Moreover, additional bands of higher molecular weight (about 60 and 80 kDa) were also detected, which could correspond to multimers of the immunoreactive band or to post-translational modifications of Prisilkin-39 (supplemental Fig. 2) as tested previously for Caspartin (35). Similarly, this banding pattern was also observed in the results of Western blotting analysis of Prisilkin-39 in different tissues. As shown in Fig. 6*D*, Prisilkin-39 mainly exists in the mantle, extrapallial fluids, and homolymph, and some is detected in the viscus. The presence of native Prisilkin-39 in the mantle, extrapallial fluid, and the homolymph meanwhile indicated the probable route of protein transportation (from the mantle tissue to the extrapallial fluid through the homolymph) before Prisilkin-39 had been occluded within the mineralized prisms.

Chitin-binding Ability of Prisilkin-39—Framework proteins are suggested to interact with chitin, a major insoluble component of the organic framework according to the models proposed by Weiner and co-workers (51–53). In support of the notion that Prisilkin-39 serves a structural role in the formation of the framework during shell growth, a chitin-binding assay was conducted. In the assay, a solution of Prisilkin-39 or BSA was incubated with powdered chitin, and the insoluble mixture was successively washed with distilled water, saline, and a hot denaturing solution. Each washing was put on SDS-PAGE (Fig. 7). BSA as a negative control was completely washed out with water and saline, whereas no band could be detected in the SDS washing. On the other hand, Prisilkin-39 could not be eluted with water and saline but with the SDS-denaturing solution, which is consistent with our previous finding that Prisilkin-39 could only be detected in the EISM fractions after being treated with similar denaturing solution at high temperature (Fig. 6). These results revealed that Prisilkin-39 could bind tightly to chitin, and with this capacity, it may therefore serve as a framework constituent participating in the shell formation.

Immunofluorescence Staining—To reveal the microstructural distribution of native Prisilkin-39 within decalcified shells, sections of the sample were immunolabeled with the anti-Prisilkin-39 antibodies. The cross-section of the shell of *P. fucata* exhibits a characteristic bilayer structure, with a prismatic texture of long, thin calcitic prisms (Fig. 8, *A* and *C, upper compartment*) and a nacreous texture of flat aragonite tablets (Fig. 8*A*, *lower compartment*). Additionally, an organic sheet (40 μm thickness) is sandwiched between the nacre and the prismatic layer. Because of its unique interfacial location, this sheet is considered to play a significant role in the transition process of the two layers with different crystal phases. The *in situ* labeling results of the same sample, which was viewed under white light (Fig. 8*A*) and epifluorescent light (Fig. 8*B*), respectively, confirmed the prism-specific location of Prisilkin-39. The positive signal was the most intense in the organic sheet, perpendicular to the axis of the prisms (Fig. 8*D*, *arrows*), as well as in the organic sheaths around the prisms, in which the main constituent is chitin (54, 55) (Fig. 8*D*, *white arrowheads*). No staining was observed in controls using preimmune serum (Fig. 8*C*). To our knowledge, Prisilkin-39 is the first matrix protein detected to be occluded in the organic sheet. This also indicates another role of this protein, namely that Prisilkin-39 should not only be a structural matrix protein to bind chitin but also might be a regulatory factor affecting crystalline deposition.

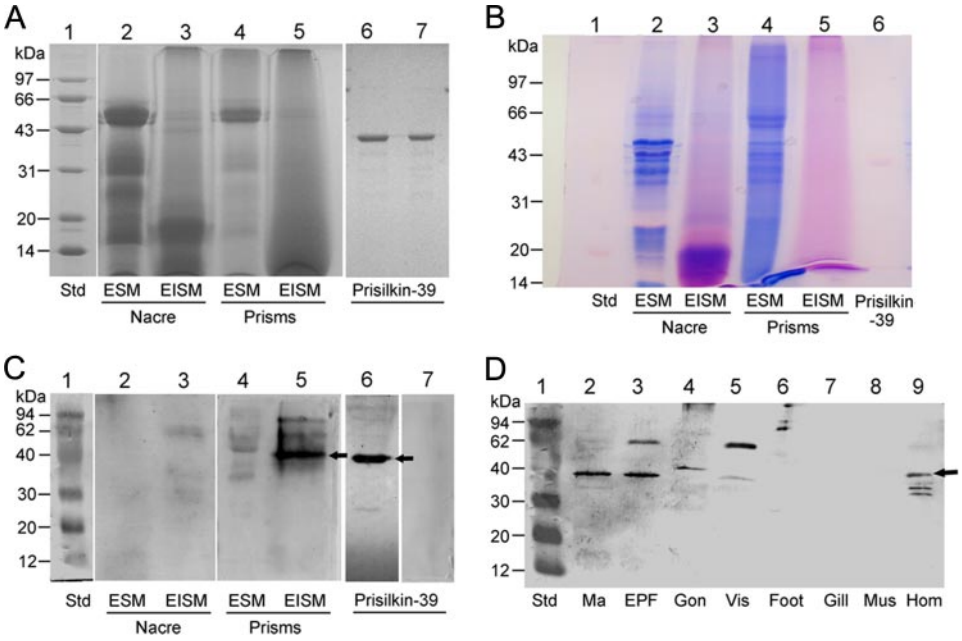

FIGURE 6. **Presence of Prisilkin-39 in specific shell layer and various tissues of *P. fucata*.** Prisilkin-39 was characterized in EDTA extracts of separated nacre and prisms of the shell on 12% SDS-polyacrylamide gels (*A* and *B*) and Western blots (*C*). The gels were stained by Coomassie Blue (*A*) and the carbocyanine dye Stains-All (*B*). *Lane 1,* molecular weight standards (*Std*); *lane 2,* EDTA-soluble matrix of the nacre; *lane 3,* the denatured fraction of the EDTA-insoluble matrix of the nacre; *lane 4,* EDTA-soluble matrix of the calcitic prisms; *lane 5,* the denatured fraction of the EDTA-insoluble matrix of the calcitic prisms; *lanes 6* and *7,* recombinant Prisilkin-39. *C,* Western blotting after electrotransfer to polyvinylidene difluoride membrane. *Lanes 1–6* were incubated with the anti-Prisilkin-39 antiserum (dilution 1:10,000), and *lane 7* was incubated with the preserum as a negative control. The *arrows* (on the *right side* of the lanes) indicate the position of the Prisilkin-39 immunoreactive band. Prisilkin-39 is mainly present in the EDTA-insoluble matrix of the calcitic prisms. *D,* Western blotting to analyze the tissue distribution pattern of Prisilkin-39. *Lane 1,* molecular weight standards (*Std*); *lane 2,* mantle (*Ma*); *lane 3,* extrapallial fluid (*EPF*); *lane 4,* gonad (*Gon*); *lane 5,* viscus (*Vis*); *lane 6,* foot; *lane 7,* gill; *lane 8,* muscle (*Mus*); *lane 9,* homolymph (*Hom*).

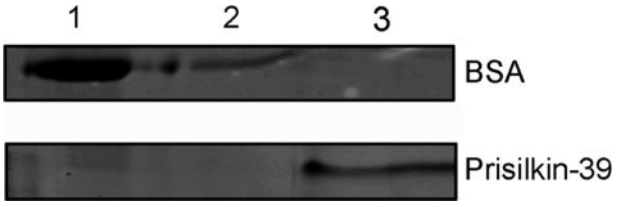

FIGURE 7. **Chitin binding assay for Prisilkin-39.** The gel was run under reducing conditions and stained by Coomassie Blue. *Lane 1,* water washings; *lane 2,* 0.2 M NaCl washings; *lane 3,* extract with SDS/β-mercaptoethanol for 10 min at 100 °C. Prisilkin-39 could only be eluted with the SDS-denaturing solution. BSA is included as a negative control.

In Vivo Investigation of the Effect of Prisilkin-39 in Mineralization—To further explore the role of Prisilkin-39 in shell biomineralization and explain why it is densely localized in the organic sheet, an *in vivo* antibody inhibition assay was performed. Affinity-purified antibodies were injected into the extrapallial fluid of *P. fucata* to disrupt the physiological functions of Prisilkin-39. Compared with the untreated group (Fig. 9, *A* and *B*), the surface of the nacre lamellae in the low dosage anti-Prisilkin-39 injected group became ragged and disordered (Fig. 9, *C* and *D*). The aberrant texture was characterized by the random accumulation of crystals on the original tablet (Fig. 9*D*, *black arrow*), disturbing the stair-like growth pattern of the inner shell. This abnormal phenomenon turned out to be more significant in the high dosage group (Fig. 9, *E* and *F*), where thickened irregular tablets were coalesced and linked together, making the boundaries obscure and fused. In addition, the chemical composition analysis by energy-dispersive x-ray spectroscopy showed that the irregular precipitations were composed of carbon, oxygen, and calcium (Fig. 9*K*). In contrast, the nacre lamellae of the preimmune-treated group kept a normal shape and smooth surfaces (Fig. 9, *G–J*). These observations revealed that large amounts of calcium carbonate could be anomalously deposited from the extrapallial fluid as a result of the suppression of the normal physiological functions of native Prisilkin-39, suggesting that Prisilkin-39 should act as an indispensable negative regulator of aragonite growth to prevent its ectopic precipitation during shell mineralization.

In Vitro Crystallization in the Presence of Prisilkin-39—To elucidate the effect of Prisilkin-39 on the growth of calcium carbonate crystals, two individual *in vitro* crystallization assays, testing the formation of aragonite and calcite, respectively, were established. In the crystalline system for aragonite precipitation, a high Mg^{2+} content (50 mM) was introduced to imitate the composition of the extrapallial fluids of *P. fucata*. First, in the control experiments performed with the filtrate (data not shown) or BSA, large needle-shaped crystals were preferentially formed, together with a number of small rod-like polyhedral crystals (Fig. 10, *A* and *B*). Raman analysis confirmed the aragonitic nature of the former crystal and its favorable stability, as visualized by a distinct sharp peak at 1085 cm^{-1} (*upper spectra*), whereas the small crystals showed a broad peak with low intensity at 1085 cm^{-1} (*lower spectra*), indicating the presence of low crystallinity deposits (Fig. 10*P*). On the other hand, in the presence of Prisilkin-39 at a concentration of 30 μg/ml, aragonite growth was completely suppressed, and no other typical calcium carbonate crystals were observed (Fig. 10, *C* and *D*). At higher magnification, these various shaped structures are obvious (Fig. 10*E*). In particular, samples were still subject to the deposition of mostly 100–200-nm spherules, together with clusters of amorphous gel-like aggregates. Raman spectra revealed that the amorphous deposits under this condition are not the typical aragonite or calcite, as shown by a low intensity peak at 1085 cm^{-1} (Fig. 10*Q*, *lower spectra*). Meanwhile, the lower concentration of Prisilkin-39 (15 μg/ml) caused the formation of vaterite crystals, each ~20 μm in size (Fig. 10, *F, G,* and *Q, upper spectra*), instead of the complete inhibition of aragonite growth.

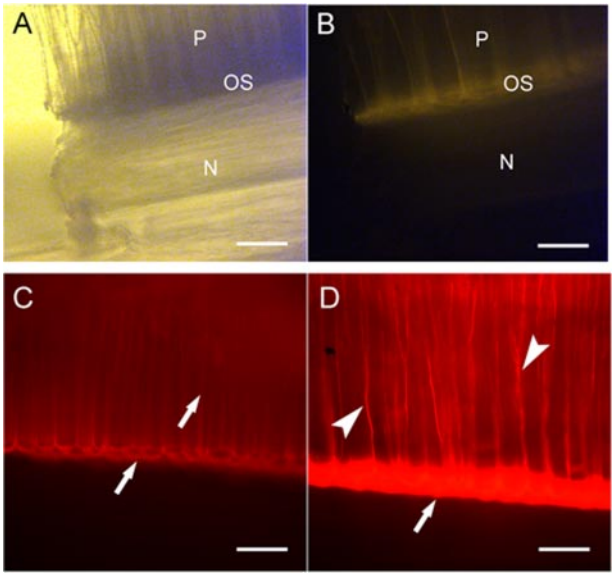

FIGURE 8. **Immunofluorescence localization of native Prisilkin-39 in cross-section of the shell of *P. fucata*.** Normal shell was fixed, decalcified, and incubated with anti-Prisilkin-39 antiserum (*A, B,* and *D*) or normal rabbit preimmune serum (*C*). The *upper compartment* is the prismatic layer, and the *lower compartment* is the nacre. For technical details, see "Experimental Procedures." *A,* differential interference contrast microscopy image of the fractured terminal of a sample stained with anti-Prisilkin-39. *B,* corresponding image of *A* visualized by fluorescence microscopy. *P,* prismatic layer; *OS,* organic sheet; *N,* nacreous layer. *C,* control sample stained with preimmune serum. The *white arrows* indicate no positive signal was detected in the organic sheet or in the prismatic sheath. *D,* sample stained with anti-Prisilkin-39. The *arrows* indicate the location of Prisilkin-39 in the organic sheet, and the *arrowheads* indicate Prisilkin-39 around the prisms. *Scale bars* in *A–D*, 50 μm.

The effect of Prisilkin-39 on calcite, generated from the Mg^{2+}-free crystalline system, was detected to be less significant compared with that on aragonite, as it only resulted in a change in crystal morphology (Fig. 10, *J–O* and *S*). Different from the aragonitic system, typical calcite crystals could be deposited normally from the saturated solution, despite the presence of Prisilkin-39 even at a quite high concentration of 50 μg/ml (Fig. 10, *N* and *O*). However, the morphology of calcite, especially on the edges and corners, was etched in a concentration-dependent manner, whereas the crystals obtained in control experiments performed with the filtrate (data not shown) or BSA (Fig. 10, *H, I,* and *R*) were the typical rhombohedra of calcite with smooth crystal faces.

To recapitulate, Prisilkin-39, as a basic matrix protein of the prismatic layer and organic sheet, exhibits a much stronger inhibitory capacity on the *in vitro* crystallization of aragonite than that of calcite. We inferred that Prisilkin-39, in cooperation with other acidic nucleating proteins, may play an important role in the passive process of calcite precipitation from the Mg^{2+}-containing extrapallial fluid for the prismatic layer mineralization, and may also have a role in the process of crystalline transition between the two distinct layers, probably by inhibiting aragonite precipitation at the growing shell edge of the prismatic layer.

In Vitro Inhibitory Activity on Calcium Carbonate Precipitation and Crystal Binding Activity—A series of precipitation experiments with or without Prisilkin-39 were performed. The effect of Prisilkin-39 on the rate of precipitation of calcium carbonate was determined by recording the increase of absorbance at 570 nm in a saturated $CaCO_3$ solution for 5 min. Addition of Prisilkin-39 to the saturated $CaCO_3$ solution caused a significantly decreased rate of precipitation in a concentration-dependent manner compared with that of the control (Fig. 11*A*). In view of the inhibitory activity of Prisilkin-39 on calcium carbonate precipitation, we tested its ability to bind calcium, and its migratory behavior in calcium-dependent electrophoresis. No positive results were observed by the Stains-All method (Fig. 6*B*, *lane 6*) or the electrophoretic shift assay (data not shown), indicating that Prisilkin-39, being a basic protein, probably had no affinity for calcium. However, protein-crystal binding experiments by incubating rhodamine-labeled Prisilkin-39 with crystals revealed that fluorescence appeared only on the edges of calcite, whereas more intense fluorescence reactivity was observed on the whole surfaces of aragonite (Fig. 11, *B* and *C*). The different binding patterns of Prisilkin-39 on aragonite and calcite are in accordance with the results of *in vitro* crystallization assays. At this point, Prisilkin-39 seems to be able to affect crystal growth by direct binding to a specific surface, depending on different crystal phases and crystal faces. Taking these results together, Prisilkin-39 may thus act as a crystal-binding rather than calcium-binding protein in the process of calcium carbonate precipitation.

DISCUSSION

Information on the structure-function relationship of matrix proteins and their role in calcification may add a piece to the puzzle of how the matrix shell, a superior mechanical material, grows (56). However, relatively few shell matrix proteins have been identified and characterized and their roles in mineralization evaluated. A fundamental difficulty has been the presence of a technical obstacle that classical fractionations usually fail to isolate and purify matrix proteins, probably because of their nonstandard behaviors in gels (4). Currently, only three proteins, namely Prismalin-14, Caspartin, and Casprismin, have been identified and partially characterized from the prismatic layer of molluscs by traditional biochemical methods (13, 35). More recently, the use of molecular biology techniques allowed the identification of putative transcripts associated with mineralization. In fact, most of the fully known sequences of shell matrix were obtained via this strategy (4). Several genes are thought to be involved in prismatic layer calcification in molluscs, but only little molecular evidence has been given (24–26). Further investigations of these genes have been difficult, as recombinant proteins are quite difficult to obtain, presumably because of their excessively biased amino acid composition. In the present study, we have cloned a gene encoding a novel molluscan shell matrix protein with an apparent molecular mass of 39 kDa, as determined by SDS-PAGE. Because this protein exists in extracts of prisms of *P. fucata* and exhibits some silk-fibroin-like characteristics of the silk hydrogel component in the mineralization microenvironment (53), we chose the name Prisilkin-39.

Prisilkin-39 is the second macromolecule so far characterized in molluscs to possess a capability to bind chitin. To date, the Rebers-Riddiford chitin-binding motif is the most widely spread motif in chitin-binding proteins found in the arthropod

cuticle (57–59). However, no such domain is found in any shell matrix protein in molluscs. Therefore, a different kind of domain should be utilized for matrix proteins to bind directly to chitin. One candidate is the Gly/Tyr-rich consensus domain. In the N-terminal part of Prisilkin-39 (Fig. 1), GYS region I is characterized by 10 tandem repeats of a 12-amino acid sequence GGY(G/S)GY(G/S)YGYP(T/A). To our knowledge, there are rare reports of this kind of motif arrangement in molluscs, being found thus far solely in Lustrin A and mucoperlin (3, 27). Although the significance of the repeated sequence has not been clarified, it may be related to the regular arrangement of atoms to the repeated structure of polymers in the insoluble organic framework such as chitin (13, 60). The secondary structure prediction revealed that GYS region I tends to form β-strand structure. Meanwhile, the Rebers-Riddiford chitin-binding motif and the chitin-binding domain of chitinases are also known to form β-strand structure to bind chitin (61). Also indicative is that GYS region I showed some similarity with the other chitin-binding sequence in molluscs, namely the Gly/Tyr-rich region of Prismalin-14, in respect to the Gly/Tyr arrangement. Therefore, we presume that the GYS region I of Prisilkin-39, together with the anterior hydrophobic sequence, may comprise a structural binding domain and be responsible for the direct interaction with chitin. The data presented here also provide support for the previous work that hypothesized that the Gly/Tyr-rich region might contain a novel chitin-binding motif in molluscan matrix proteins (61). Our further studies on synthesized peptides are currently in progress.

From the amino acid sequence and the hydropathy analysis (Fig. 2), Prisilkin-39 clearly possesses an amphiphilic geometry comprising an N-terminal hydrophobic and a C-terminal hydrophilic domain.

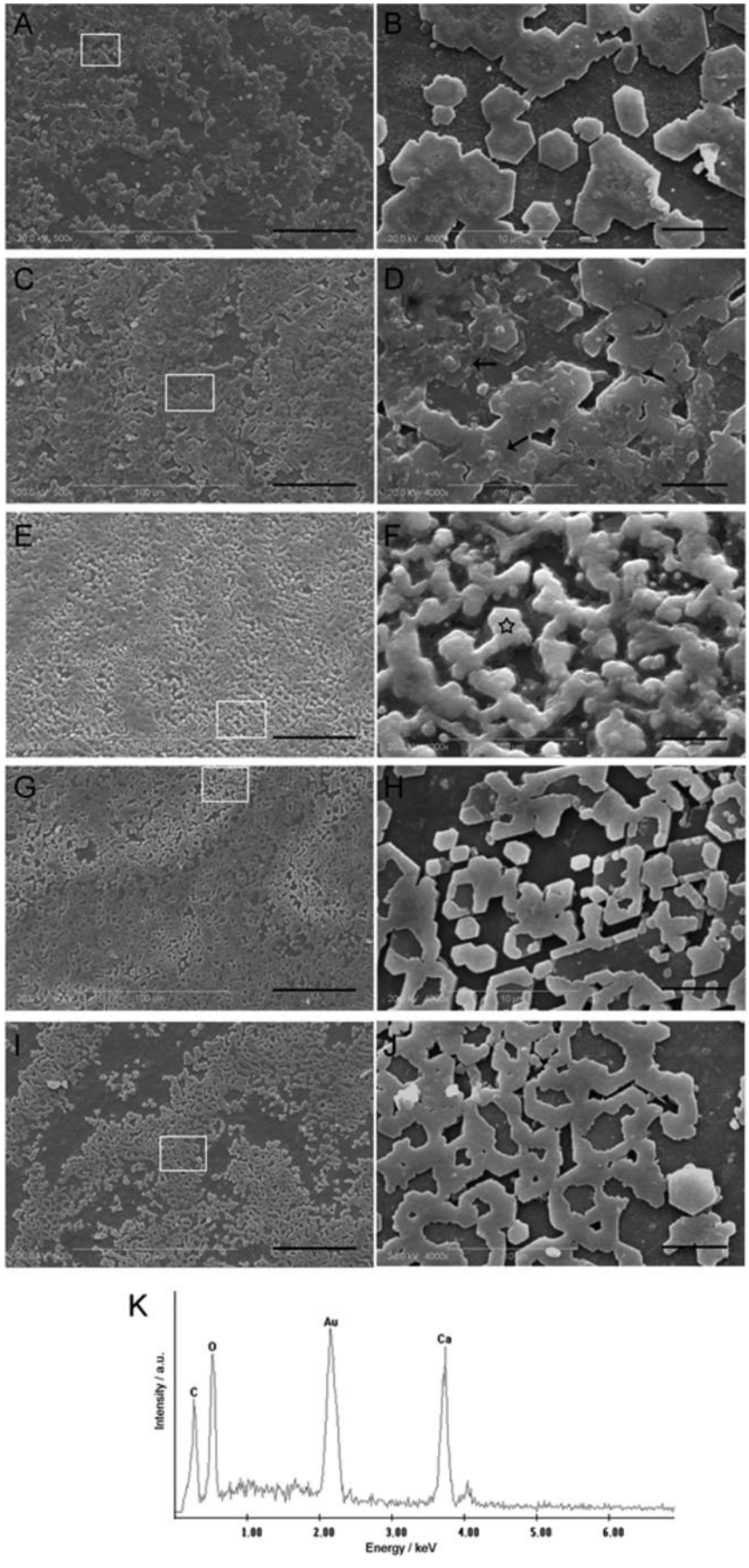

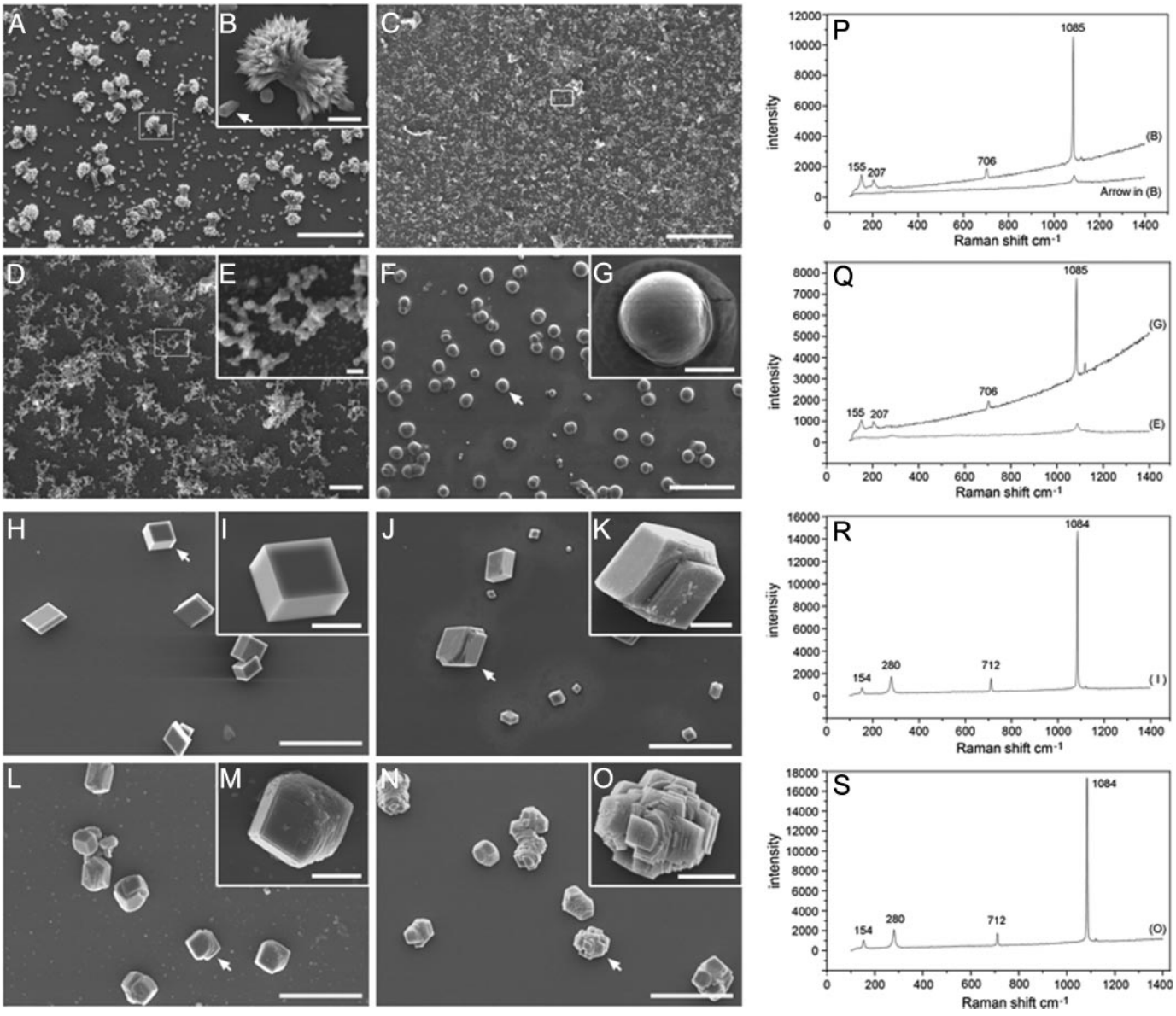

FIGURE 10. **SEM images of *in vitro* crystallization experiments in the presence of Prisilkin-39 and their Raman spectra.** The effect of Prisilkin-39 on the growth of calcium carbonate crystals were tested in two crystallization systems. *A–G,* crystallization in the presence of 50 mM Mg^{2+} for aragonite growth; *A* and *B,* crystallization with 30 μg/ml BSA as a negative control, large needle-shaped crystals (aragonites) and small rod-like crystals are *boxed* and enlarged in *B*. *C–E,* crystallization with 30 μg/ml Prisilkin-39 (*D* and *E*) are enlarged images of the *boxed part* in *C* and *D*, respectively. No aragonite crystals were formed, whereas amorphous gel-like aggregates and nano-scale spherules can be seen in *E*. *F* and *G,* crystallization with 15 μg/ml Prisilkin-39. A spherical crystal is indicated by an *arrow* in *F* and enlarged in *G*. *H–O,* crystallization in the absence of Mg^{2+} for calcite growth. Calcite crystals were grown in the presence of 30 μg/ml BSA in *H*, 10 μg/ml Prisilkin-39 in *J*, 30 μg/ml Prisilkin-39 in *L*, and 50 μg/ml Prisilkin-39 in *N*. *I, K, M,* and *O* are the enlarged images of the crystal indicated by *arrows* in *H*, *J*, *L,* and *N*, respectively. *P–S,* Raman spectra of the crystals formed in these experiments. *Scale bars,* 100 μm in *A, C,* and *F*; 50 μm in *H, J, L,* and *N*; 10 μm in *B, D, G, I, K, M,* and *O*; 1 μm in *E*.

According to a previous study of the matrix protein Ansocalcin (56) on eggshell biomineralization, this amphiphilic characteristic facilitates self-assembly, which consequently can give rise to a hydrophilic exterior surface encompassing the basic side chains in the C-terminal tail. Such a feature may then assist specific interactions with a specific acidic protein that was recruited to function as a nuclear factor, or with crystalline faces regulating crystal growth. Additionally, the predicted

FIGURE 9. **The effect of Prisilkin-39 on the growth of nacre lamellae.** In the extrapallial fluid where shell biomineralization occurs, the physiological functions of free Prisilkin-39 were inhibited by its antibody. *A,* SEM image of the inner surface of normal shell of the oyster *P. fucata*. The stair-like growth pattern of nacre can be seen. *B,* enlargement of the box in *A* showing flat and regular tablets. *C,* SEM image of the inner surface of the shell in low dosage anti-Prisilkin-39 treated group. The stair-like growth edge became merged. *D,* enlargement of the box in *C* showing the coarse surface and disordered arrangement of the tablets. Random accumulation of crystals on the original tablet can be seen (*arrows*). *E,* SEM image of the inner surface of the shell in high dosage anti-Prisilkin-39 treated group. Large amounts of low crystallinity of calcium carbonate were precipitated in an uncontrolled manner. *F,* enlargement of the box in *E* showing the thickened and irregular tablets. *G,* SEM image of the inner surface of the shell in low dosage preimmune serum treated group. *H,* enlargement of the box in *G* showing the normal shape and smooth surface of the tablets. *I,* SEM image of the inner surface of the shell in high dosage preimmune serum treated group. *J,* enlargement of the box in *I*. *K,* energy-dispersive x-ray spectroscopy analysis of the deposition (*asterisk*) in *F*. *Scale bars,* 50 μm in *A, C, E, G,* and *I*; 5 μm in *B, D, F, H,* and *J*.

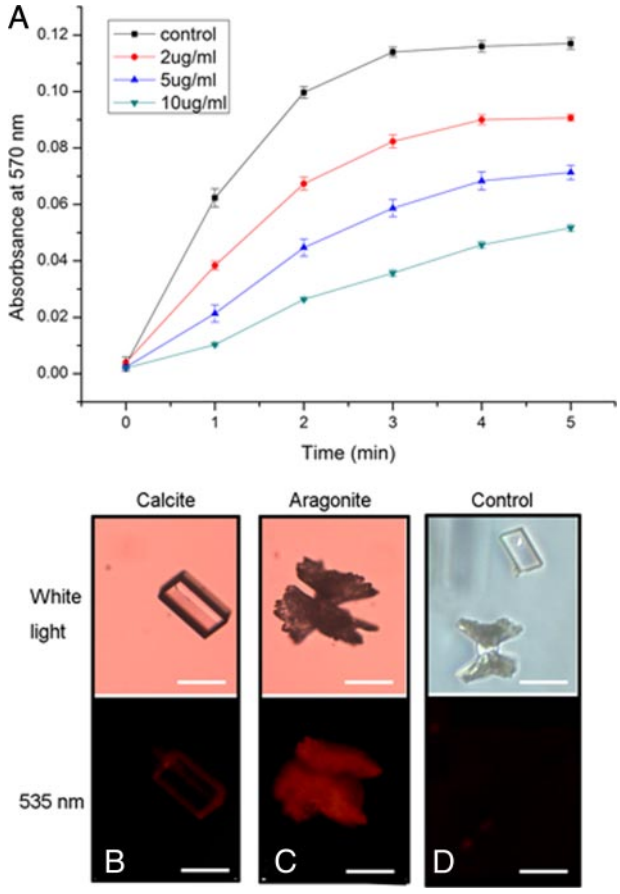

FIGURE 11. **Inhibitory activity of Prisilkin-39 on calcium carbonate precipitation.** *A*, changes in the turbidity of the assayed solutions are shown. ●, 2 μg/ml Prisilkin-39; ▲, 5 μg/ml Prisilkin-39; ▼, 10 μg/ml Prisilkin-39. In the *in vitro* crystal-protein binding experiment, Prisilkin-39 showed different binding patterns on single calcite (*B*) and aragonite (*C*). No fluorescence was detected when equimolar BSA and rhodamine were added (*D*). *Scale bars* in *B–D*, 20 μm.

analysis that GYS region II is more sensitive to post-translational modifications indicates a quite exquisite structure of this molecule is required for effective matrix-matrix or matrix-mineral interactions. On the other hand, the secondary structure showed that GYS region II is mainly made up of random coil, which generally contributes to the flexibility and elasticity of the molecular conformation. We suppose that this feature is highly favorable to the regulatory activities of Prisilkin-39 in crystallization.

Expression of *Prisilkin-39* was detected only in the mantle edge but not in the mantle pallium nor other tissues (Fig. 4*A*), indicating the involvement of Prisilkin-39 in calcitic prismatic layer formation during shell growth. This expression profile was further evidenced by the results of immunofluorescence staining *in situ* and immunodetection *in vitro*. All the results presented above are direct genetic and biochemical evidence that basic matrix proteins can also take part in the prismatic layer construction, even though they had never been successfully extracted before. A striking distribution pattern of native Prisilkin-39 in the shell was observed in Fig. 8. Before this study, matrix protein in the organic sheet had never been identified and characterized in molluscs. Hence, detection of Prisilkin-39 in the organic sheet, where an abrupt crystalline transition between aragonite and calcite occurs, pointed at another possible role of Prisilkin-39 in the process of shell biomineralization. It is well known that multifunction is a common characteristic of many shell matrix proteins such as Lustrin A (3), MSI60 (5), and nacrein (6), and we infer that Prisilkin-39 shares it. In support of this notion, its biomineralization function was tested, using both *in vivo* antibody inhibition assay and *in vitro* precipitation of calcium carbonate. To investigate the crystal precipitation process, the ionic composition of the extrapallial fluid of marine molluscs, with a high Mg^{2+} content (50 mM) relative to Ca^{2+} (10 mM) (62), must be taken into consideration. In solution, Mg^{2+} is harmful to calcite precipitation; this is why aragonite crystals become dominant in Mg^{2+}-rich solutions (23). Consequently, for an efficient process of calcitic prismatic layer calcification, some regulatory factors are required to override this spontaneous condition to form calcite. Hence, we infer that Prisilkin-39 is one of these molecules that act as a safeguard of calcite growth, as our *in vitro* results coincide well with the *in vivo* observation that Prisilkin-39 showed a powerful inhibitory capacity on the precipitation of aragonite but not of calcite. We should note that the two aspects that Prisilkin-39 takes part in, namely intercolumnar framework building and aragonite growth inhibition, are thoroughly faithful to the construction of the prismatic layer. In addition, crystal binding experiments (Fig. 11) further revealed a different binding profile for Prisilkin-39 on aragonite and calcite. However, the regulation of crystal growth should be more subtle and complex, and the minute manner by which Prisilkin-39 forbids aragonite formation has yet to be elucidated.

How are the calcitic prisms in the growing shell edge of *P. fucata* formed? Although the mechanism for growth of the prism, especially for the initiation stage beneath the inner periostracum, is still unclear, our study presented here provides important clues for these complicated physiological processes. We do believe that both acidic and basic matrix proteins are required to function in a cooperative way to fulfill this work. In the absence of a comprehensive model for the prismatic layer construction, any suggestion for the role of Prisilkin-39 must be tentative. First, basic matrix proteins bind tightly to a chitinous framework to form a regular platform for crystal precipitation. Second, some proteins such as Prisilkin-39, because of their amphiphilic character, also play an interfacial role by linking together the framework and acidic matrix proteins, which are sequestered by basic residues of Prisilkin-39. At the same time, acidic proteins nucleate calcite on the condition that the spontaneous nucleation and growth of aragonite are prohibited by Prisilkin-39 on the same mineralization site. Another important point to mention is that the property and function of Prisilkin-39 we presented here are in remarkable accordance with that of the silk-like proteins in the shell, which are widely thought to possess three basic roles in biomineralization as follows: 1) pre-filling the microenvironment formed by two layers of β-chitin; 2) some of these molecules are finally trapped into the mineralized framework with shell growth; and 3) they may act as an inhibitor and help prevent uncontrolled crystallization at unnecessary nucleation sites. Although silk-like proteins have not been characterized in

prisms before this study, we tentatively infer that the suggested model for nacre mineralization by Addadi *et al.* (53) is also to some extent comparable with the prismatic layer biomineralization in respect to some fundamental steps, *i.e.* the chitinous framework construction and crystal growth termination. Thus, according to Marin *et al.* (4), "the classical paradigm in molluscan shell biomineralization was to consider that the control of shell synthesis was performed primarily by two antagonistic mechanisms, crystal nucleation and growth inhibition." We think that Prisilkin-39 is the latter.

In conclusion, based on the structural and functional characteristics of Prisilkin-39, we propose a suggested molecular model for this protein. This molecule has four functional parts. GYS region I, together with the alanine-rich hydrophobic region, comprise a structural domain. They form a β-strand structure and help bind directly to chitin, and thus are mainly responsible for the toughness of the shell. GYS region II and the basic tail in the C terminus are predicted to be more flexible in their secondary structure, and they may bind to specific crystal surfaces or acidic matrix proteins neatly regulating mineral precipitation by means of specific growth inhibition. Further studies on the structure-function relationship, as well as antisense RNA assays, are required to understand the physiological function of Prisilkin-39 in the formation of the prismatic layer of *P. fucata.*

Acknowledgments—Special thanks are given to Professor Steve Weiner (Dept. of Structural Biology, Weizmann Institute of Science, Rehovot 76100, Israel) for helpful suggestions on this work and to Xianying Tan and Zhongxin Wei for their help in the manuscript preparation.

REFERENCES

1. Lowenstam, H. A., and Weiner, S. (1989) *On Biomineralization*, Oxford University Press, New York
2. Belcher, A. M., Wu, X. H., Christensen, R. J., Hansma, P. K., Stucky, G. D., and Morse, D. E. (1996) *Nature* **381,** 56–58
3. Shen, X., Belcher, A. M., Hansma, P. K., Stucky, G. D., and Morse, D. E. (1997) *J. Biol. Chem.* **272,** 32472–32481
4. Marin, F., Luquet, G., Marie, B., and Medakovic, D. (2008) *Curr. Top. Dev. Biol.* **80,** 209–276
5. Sudo, S., Fujikawa, T., Nagakura, T., Ohkubo, T., Sakaguchi, K., Tanaka, M., Nakashima, K., and Takahashi, T. (1997) *Nature* **387,** 563–564
6. Miyamoto, H., Miyashita, T., Okushima, M., Nakano, S., Morita, T., and Matsushiro, A. (1996) *Proc. Natl. Acad. Sci. U. S. A.* **93,** 9657–9660
7. Zhang, C., and Zhang, R. (2006) *Mar. Biotechnol.* (*N. Y.*) **8,** 572–586
8. Marin, F., and Luquet, G. (2004) *C. R. Palevol.* **3,** 469–492
9. Matsushiro, A., and Miyashita, T. (2004) *J. Bone Miner. Metab.* **22,** 163–169
10. Berman, A., Addadi, L., and Weiner, S. (1988) *Nature* **331,** 546–548
11. Weiner, S., and Addadi, L. (1991) *Trends Biochem. Sci.* **16,** 252–256
12. Tsukamoto, D., Sarashina, I., and Endo, K. (2004) *Biochem. Biophys. Res. Commun.* **320,** 1175–1180
13. Suzuki, M., Murayama, E., Inoue, H., Ozaki, N., Tohse, H., Kogure, T., and Nagasawa, H. (2004) *Biochem. J.* **382,** 205–213
14. Sarashina, I., and Endo, K. (2001) *Mar. Biotechnol.* (*N. Y.*) **3,** 362–369
15. Hasegawa, Y., and Uchiyama, K. (2005) *Fish. Sci.* (*Tokyo*) **71,** 1174–1178
16. Gotliv, B. A., Kessler, N., Sumerel, J. L., Morse, D. E., Tuross, N., Addadi, L., and Weiner, S. (2005) *ChemBioChem* **6,** 304–314
17. Hare, P. E. (1963) *Science* **139,** 216–217
18. Weiner, S., and Hood, L. (1975) *Science* **190,** 987–989
19. Weiner, S. (1983) *Biochemistry* (*Mosc.*) **22,** 4139–4145
20. Gotliv, B. A., Addadi, L., and Weiner, S. (2003) *ChemBioChem.* **4,** 522–529
21. Falini, G., Albeck, S., Weiner, S., and Addadi, L. (1996) *Science* **271,** 67–69
22. Feng, Q. L., Pu, G., Pei, Y., Cui, F. Z., Li, H. D., and Kim, T. N. (2000) *J. Cryst. Growth* **216,** 459–465
23. Takeuchi, T., Sarashina, I., Iijima, M., and Endo, K. (2008) *FEBS Lett.* **582,** 591–596
24. Yano, M., Nagai, K., Morimoto, K., and Miyamoto, H. (2006) *Comp. Biochem. Physiol. B. Biochem. Mol. Biol.* **144,** 254–262
25. Zhang, C., Xie, L., Huang, J., Liu, X., and Zhang, R. (2006) *Biochem. Biophys. Res. Commun.* **344,** 735–740
26. Nagai, K., Yano, M., Morimoto, K., and Miyamoto, H. (2007) *Comp. Biochem. Physiol. B. Biochem. Mol. Biol.* **146,** 207–214
27. Marin, F., Corstjens, P., de Gaulejac, B., de Vrind-De Jong, E., and Westbroek, P. (2000) *J. Biol. Chem.* **275,** 20667–20675
28. Marin, F., and Luquet, G. (2005) *L. Mater. Sci. Eng., C.* **25,** 105–111
29. Huang, W., Yao, B., Sun, L., Pu, R., Wang, L., and Zhang, R. (2001) *Life Sci.* **68,** 1727–1734
30. Fan, X., Hou, J., Chen, X., Chaudhry, F., Staiger, C. J., and Ren, H. (2004) *Plant Physiol.* **136,** 3979–3989
31. Clark, M. F., and Adams, A. N. (1977) *J. Gen. Virol.* **34,** 475–483
32. Nudelman, F., Gotliv, B. A., Addadi, L., and Weiner, S. (2006) *J. Struct. Biol.* **153,** 176–187
33. Inoue, H., Ozaki, N., and Nagasawa, H. (2001) *Biosci. Biotechnol. Biochem.* **65,** 1840–1848
34. Xu, G., Yao, N., Aksay, I. A., and Groves, J. T. (1998) *J. Am. Chem. Soc.* **120,** 11977–11985
35. Marin, F., Amons, R., Guichard, N., Stigter, M., Hecker, A., Luquet, G., Layrolle, P., Alcaraz, G., Riondet, C., and Westbroek, P. (2005) *J. Biol. Chem.* **280,** 33895–33908
36. Li, S., Xie, L., Zhang, C., Zhang, Y., Gu, M., and Zhang, R. (2004) *Comp. Biochem. Physiol. B. Biochem. Mol. Biol.* **138,** 235–243
37. Burgess, W. H., Jemiolo, D. K., and Kretsinger, R. H. (1980) *Biochim. Biophys. Acta* **623,** 257–270
38. Ma, Z., Huang, J., Sun, J., Wang, G., Li, C., Xie, L., and Zhang, R. (2007) *J. Biol. Chem.* **282,** 23253–23263
39. Kozak, M. (1989) *J. Cell Biol.* **108,** 229–241
40. Kozak, M. (1996) *Mamm. Genome* **7,** 563–574
41. Wada, K. (1966) *Bull. Natl. Pearl Res. Lab.* **20,** 2209–2213
42. Zhang, Y., Xie, L., Meng, Q., Jiang, T., Pu, R., Chen, L., and Zhang, R. (2003) *Comp. Biochem. Physiol. B. Biochem. Mol. Biol.* **135,** 565–573
43. Hansen, J. E., Lund, O., Tolstrup, N., Gooley, A. A., Williams, K. L., and Brunak, S. (1998) *Glycoconj. J.* **15,** 115–130
44. Blom, N., Gammeltoft, S., and Brunak, S. (1999) *J. Mol. Biol.* **294,** 1351–1362
45. Altschul, S. F., Madden, T. L., Schaffer, A. A., Zhang, J., Zhang, Z., Miller, W., and Lipman, D. J. (1997) *Nucleic Acids Res.* **25,** 3389–3402
46. Suzuki, N., Nadano, D., Paria, B. C., Kupriyanov, S., Sugihara, K., and Fukuda, M. N. (2000) *Endocrinology* **141,** 4247–4254
47. Mann, S. (ed) (2001) *Biomineralization. Principles and Concepts in Bioinorganic Materials Chemistry*, pp. 89–119, Oxford University Press, Oxford
48. Yan, Z., Jing, G., Gong, N., Li, C., Zhou, Y., Xie, L., and Zhang, R. (2007) *Biomacromolecules* **8,** 3597–3601
49. Pereira-Mouries, L., Almeida, M. J., Ribeiro, C., Peduzzi, J., Barthelemy, M., Milet, C., and Lopez, E. (2002) *Eur. J. Biochem.* **269,** 4994–5003
50. Bowen, C. E., and Tang, H. (1996) *Comp. Biochem. Physiol. A* **115,** 269–275
51. Weiner, S., Traub, W., and Parker, S. B. (1984) *Philos. Trans. Royal Soc. Lond. B Biol. Sci.* **304,** 425–433
52. Levi-Kalisman, Y., Falini, G., Addadi, L., and Weiner, S. (2001) *J. Struct. Biol.* **135,** 8–17
53. Addadi, L., Joester, D., Nudelman, F., and Weiner, S. (2006) *Chem. Eur. J.* **12,** 980–987

54. Dauphin, Y. (2003) *J. Biol. Chem.* **278,** 15168–15177
55. Suzuki, M., Sakuda, S., and Nagasawa, H. (2007) *Biosci. Biotechnol. Biochem.* **71,** 1735–1744
56. Lakshminarayanan, R., Valiyaveettil, S., Rao, V. S., and Kini, R. M. (2003) *J. Biol. Chem.* **278,** 2928–2936
57. Andersen, S. O. (1998) *Comp. Biochem. Physiol. A* **121,** 375–383
58. Faircloth, L. M., and Shafer, T. H. (2007) *Comp. Biochem. Physiol. B. Biochem. Mol. Biol.* **146,** 370–383
59. Andersen, S. O. (2000) *Insect Biochem. Mol. Biol.* **30,** 569–577
60. Addadi, L., Weiner, S., and Geva, M. (2001) *Z. Kardiol.* **90,** 92–98
61. Suzuki, M., and Nagasawa, H. (2007) *FEBS J.* **274,** 5158–5166
62. Wada, K., and Fujinuki, T. (1976) in *The Mechanisms of Mineralization in the Invertebrates and Plants* (Watabe, N., and Wilbur, K. M., eds) pp. 175–190, University of South Carolina Press, Columbia